Heliyon 5 (2019) e01693

Contents lists available at ScienceDirect

Heliyon

journal homepage: www.heliyon.com

Uranyl nitrate crystallizer performance with changing solution level

Igor S. Nadezhdin [a,*], Alexandr I. Gozhimov [a], Alexey G. Goryunov [a], Simone Colombo [b], Flavio Manenti [b]

[a] National Research Tomsk Polytechnic University, School of Nuclear Science & Engineering, Lenin Avenue 30, 634050, Tomsk, Russia
[b] Politecnico di Milano, Dept. di Chimica, Materiali e Ingegneria Chimica "Giulio Natta", Piazza Leonardo da Vinci 32, 20133, Milano, Italy

ARTICLE INFO

Keywords:
Applied mathematics
Chemical engineering

ABSTRACT

This manuscript described a dynamic simulation of uranyl nitrate crystallization in a linear crystallizer. Furthermore, a mathematical model of the crystallizer supply system was developed with a related control algorithm; the model contained two piston feeders. The results showed the crystallization process's sensitivity to the solution level in the crystallizer. An expression for calculating the performance of the crystallizer was proposed. That expression allowed us to understand that the accuracy of the liquid phase level (to avoid the crystallizer's performance decreasing by more than 5%) should be in the range of ±4% of the crystallization section height. For this, we developed a control algorithm for the supply system to support operability. This algorithm allowed us to maintain a specified level of mother solution in the crystallization area and provided an asynchronous operation mode for the piston batchers. Furthermore, this paper described how the developed mathematical model and the proposed control system, i.e., the envisaged recommendations, can be used to optimize the process during the design and adjustment of equipment.

1. Introduction

Nowadays, nuclear energy is regaining attention thanks to greatly increasing energy demands across the world [1]. However, one of the key issues in making nuclear energy sources appealing is the disposal of the spent nuclear fuel (SNF). The aim of this manuscript is to present the work performed by the Russian State Atomic Energy Corporation "Rosatom" within the "Proryv" project, whose goal is to achieve the necessary product purity to allow for a cleaner and safer reuse of the SNF in a nuclear fuel cycle. More specifically, the manuscript presents the process design and associated process control, both approached from a mathematical modeling standpoint.

Traditionally, the strategy to reduce nuclear waste involves processing the SNF to extract reusable products; this is seen in the well-established Plutonium Uranium Reduction EXtraction (PUREX) process, which dates back to the 1950s. The idea behind this process is to extract a selection of target products from the SNF solution by means of specific organic solvents. Despite the idea being undoubtedly good, the PUREX process presents three main drawbacks: (a) it generates a significant amount of plutonium oxide waste; (b) the process requires both large equipment (i.e., tanks of a significant size) and the use of a significant quantity of reagents; and (c) the solution coming from the process might be degraded by hydrolysis and radiolysis.

An alternative to the solvent-based PUREX process is crystallization *affinage*, which has been adopted by different industries to obtain the required purity of a target product from a multicomponent solution [2]. The peculiarity of this technology is that the crystallization is considered as an additional step on top of the traditional extraction process. German scientists attempted to use crystallization *affinage* in addition to the PUREX process with the ultimate goal of purifying uranium after its separation from plutonium [3, 4]. Similar attempts were made in Japan [5]. The results of these studies showed that the separation efficiency during crystallization is not as high as those in solvent-based extraction, and that the recovery of uranium is more difficult.

Despite these weaknesses, the crystallization process might have several advantages for the PUREX process, and thus the idea to use crystallization within the PUREX process was pursued within the "Proryv" project. From a process standpoint, the first and most evident benefit relates to safety since, unlike the extraction process, crystallization does not require the use of combustible organic solvents, thus making the process inherently safer (a parameter that might become industrially and politically crucial considering the increasing societal aversion toward risky technologies). Moreover, given that crystallization can allow us to avoid some downstream processes related to solvent treatment, coupling it with the PUREX process might not just make the PUREX process safer

* Corresponding author.
E-mail address: kun9@tpu.ru (I.S. Nadezhdin).

https://doi.org/10.1016/j.heliyon.2019.e01693
Received 3 September 2018; Received in revised form 28 March 2019; Accepted 7 May 2019

Nomenclature

ΔR	crystal radius increment (m)
K_{kr}	crystal growth speed (m/s)
C^0_{UN}	concentration of uranyl nitrate in solution at 1-th cell inlet (g/L)
C_{sat}	saturation concentration of the solution (g/L)
t_{kr}	crystal transit time through cell height (s)
L	cell height (m)
i	cell number
U_{sol}	solid phase transit speed in crystallization section (m/s)
U_{liq}	liquid phase transit speed (m/s)
g	acceleration of gravity (m/s^2)
ν	liquid phase kinematic viscosity (Pa·s)
R	radius of the formed crystal (m)
ρ_{sol}	solid phase mass density (g/L)
ρ_{liq}	liquid phase mass density (g/L)
Q_{liq}	solution input flow (m^3/s)
D	crystallizer diameter (m)
C_{UN}	concentration of uranyl nitrate in solution (g/L)
C_{HNO3}	concentration of nitric acid in solution (g/L)
T	solution temperature (°C)
C^0_{HNO3}	concentration of nitric acid in solution at 1-th cell inlet (g/L)
n	number of crystallization centers
R_{in}	crystal radius at 1-th cell inlet (m)
W	solid phase volume fraction
S	sectional area (m^2)
V	volume of the grid block (m^3)
T_{tr}	crystallizer pipe temperature in cell (°C)
a_p	heat transfer coefficient from brine to pipe (W/(m^2·°C))
S_{tr}	pipe surface area in cell (m^2)
T_{wall}	brine temperature (°C)
a_g	heat transfer coefficient (W/(m^2·°C))
T_{out}	temperature at the cell outlet (°C)
m_{tr}	pipe mass in cell (g)
C_{tr}	pipe specific heat (J/(g·°C))
M_{sum}	liquid and solid phases' total mass flow in cell (g/s)
C_{sr}	solid and liquid phases' average specific heat (J/(g·°C))
T_{in}	temperature at the cell inlet (°C)
m_{sum}	solid and liquid phases' mass in cell (g)
C_{liq}	liquid phase average specific heat (J/(g·°C))
C_{sol}	solid phase average specific heat (J/(g·°C))
U_{pr}	washing solution speed (m/s)
Q_{pr}	washing solution flow (m^3/s)
$V^{bat.}_{liq.}$	mother solution volume in the batcher (m^3)
$Q^{bat.}_{liq.}$	mother solution volume flow supplied to batcher (m^3/s)
$v^{bat.}_{liq.}$	solution flow rate at the inlet of the batcher (m/s)
$S_{b.p.6}$	branch pipe №6 sectional area (m^2)
$R_{b.p.6}$	branch pipe №6 radius (m)
N_{step}	number of steps done by the stepper motor within 1 s
T_{FIM}	pulse frequency modulation period (ms)
Δh_{piston}	piston movement of one step of the motor (m)
S_{piston}	piston base area (m^2)
r_{piston}	piston radius (m)
r_{hole5}	hole №5 radius (m)
r_{hole6}	hole №6 radius (m)
C_i	i-th component concentration in mother solution in batcher (i = U, Pu, Np, HNO_3) (g/L)
$C^{bat.}_i$	i-th component concentration in mother solution at batcher inlet (g/L)
m_{cryst}	outlet mass flow of crystals (g)
lev_{liq}	fullness of the crystallization section (%)

but also greener. Furthermore, thanks to this new approach, the overall process can be simplified and the volume of radioactive liquid material required can be remarkably reduced, thus leading to a decrease in both investment costs (associated with reductions in installation size and construction time) and operations costs.

Despite the great potential (in terms of sustainability) that the crystallization technique might bring to the PUREX process, it is evident from the scientific literature that there are still some key aspects that require further investigation and development in order for this novel (technological) approach for SNF reprocessing to be consolidated and made industrially viable. For instance, in Japan there are two streams of research, namely, the New EXtraction system for True recovery (NEXT) process, and the uranium and plutonium mutual crystallization process.

The NEXT process is based on the PUREX concept, yet was developed for fast neutron reactors [6]. With this method, 70% of uranium is recovered by crystallization, thus reducing the inlet mass flow rate with respect to the extraction process (i.e., PUREX). Conversely, the uranium and plutonium mutual crystallization process is based on experimental data that indicate that the hexavalent plutonium crystallizes with uranyl nitrate in the presence of nitric acid [7, 8]. These latter experimental studies allowed us to develop a method of pure uranium and plutonium extraction (by crystallization) with a higher uranium concentration than that in the PUREX process.

Unfortunately, the crystallization process is difficult to achieve and manage because it requires both strict compliance with all safety standards and the use of a highly sophisticated technology. For these reasons, further investigations are necessary in this field to reduce both the need for complex technologies and the safety implications associated with the process (such as for hexahydrate crystals growing of uranyl nitrate and crystallization processes). Unfortunately, the high radioactivity of the SNF strongly limits the possibility of direct experimentation on its processing. Actually, in order to perform this type of experiment it is necessary to prevent people, as well as equipment, from contacting the radioactive material processed by the experimental equipment; it is also necessary to design and install a protective system, made up of both hardware and software control, to (remotely) control the experimental process during operations. Should the process deviate from its nominal, expected conditions, the protective system must automatically shut it down before it reaches undesired critical or emergency conditions. To that end, and in order for the control software to function properly (i.e., to allow for operators to control the process during operations and automatically shut it down when approaching risky operation) it is necessary to develop a suitable model of the crystallization process that allows us to build different simulations in different operating conditions, with the ultimate goal of estimating the final product quality and the associated productivity.

In order to reach that goal, one of the most important aspects is to couple the consolidated theoretical foundations with modern approaches. Among many, the main and most critical feature is the simulation of the phase equilibrium in the solution [9, 10]. However, given that measuring the thermodynamic properties of this process is extremely difficult, especially in extreme conditions (e.g., high pressure or low temperature), the only way forward is to appeal to mathematical modeling. In this respect, phase equilibrium curves could provide extremely useful information on both the characteristics of the components and the overall system. Moreover, to correctly forecast the transition phases of the process and enable the modeling of these phenomena, it is necessary to reliably determine the equilibrium phase. To that end, by taking advantage of the work performed by Veselov [11], we used an ordinary differential equations system. Moreover, cellular automata were

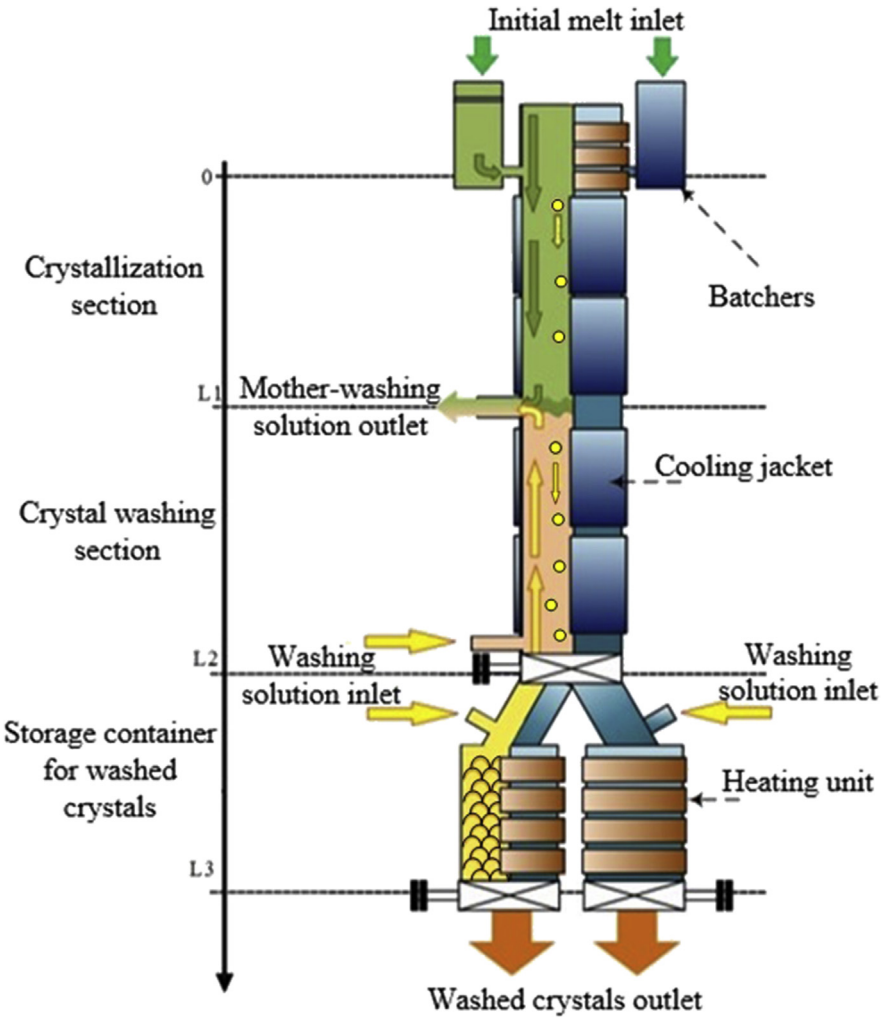

Fig. 1. Structure of a linear crystallizer.

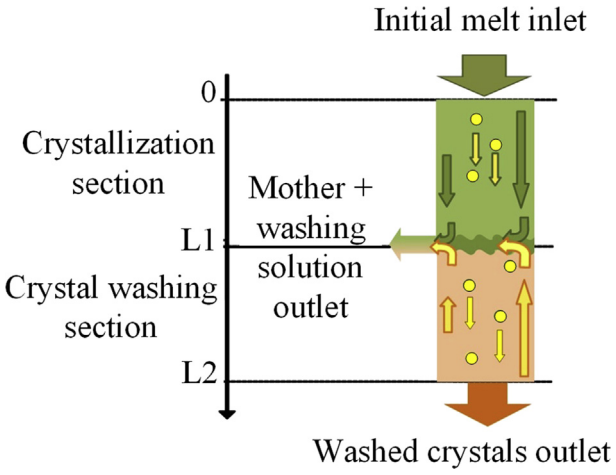

Fig. 2. Solution motion during the crystallization process.

used to model the crystal growth in a linear crystallizer [12, 13].

Given that the goal of the work was to perform virtual experiments, i.e., simulating the behavior of the PUREX process combined with crystallization, we first needed to consider the influence of the linear crystallizer on the processes. To that end, we created a mathematical model of a linear crystallizer and a piston batcher. This model was coupled with a control algorithm of the supply system to support operations, i.e., help researchers operate the experimental equipment, and (automatically) manage potential process upsets, thus preventing emergency conditions by timely automatic shutdowns. More specifically, the aim of the work was to define the sensitivity of the crystallization with respect to the level of the mother solution in the crystallization area and the batching accuracy. The resulting model seems to be sufficiently good in predicting the crystallization behavior. However, it is worth mentioning that there are still some problems with the control of the solution level in the crystallizer. This incorrect behavior seems to be ascribable to the construction complexity of the experimental equipment (i.e., the complexity of mounting the level meter devices in the crystallizer body); this generates measurement errors and leads to an additive noise in the data source (bringing to errors of the static nature). This is why efforts were devoted to better understanding the sensitivity of the crystallization process with respect to the level of the solution.

2. Theory

The structure of a linear crystallizer devoted to uranium purification is shown in Fig. 1. A crystallizer is a vertical column-type equipment. It has two piston batchers positioned at the two sides of its top, a vertical column, and a cumulative double chamber unit at the bottom. In fact, the working volume of the crystallizer can be divided into three areas [11], namely, the crystallization area, the washing area, and the cumulative area. The process is carried out by feeding the uranyl nitrate solution at

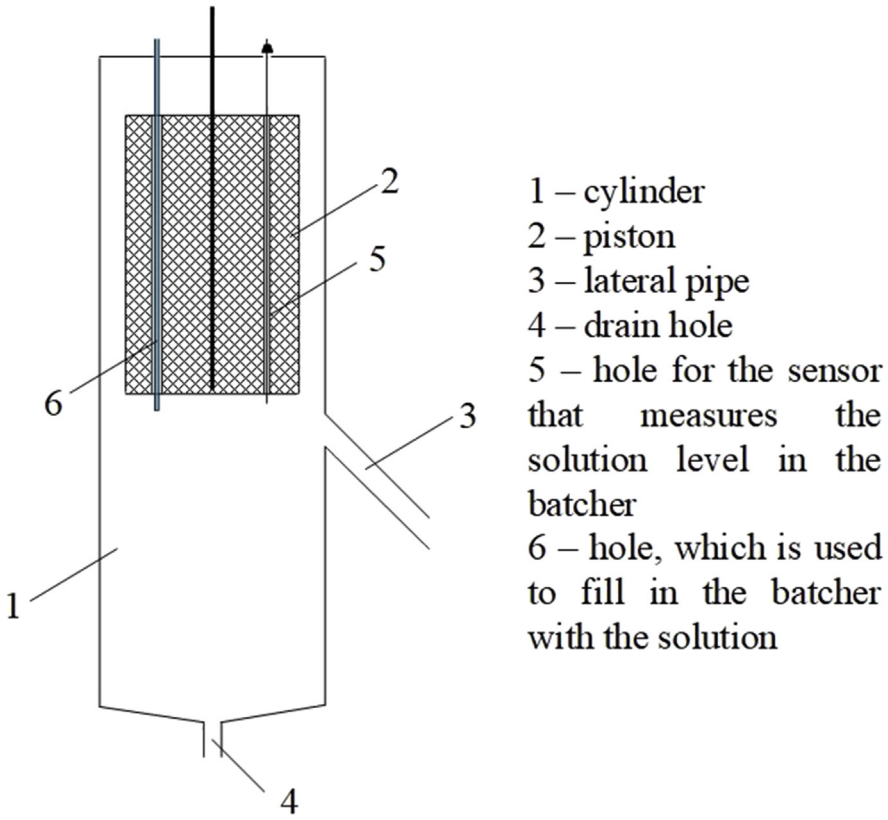

Fig. 3. Batcher schematic.

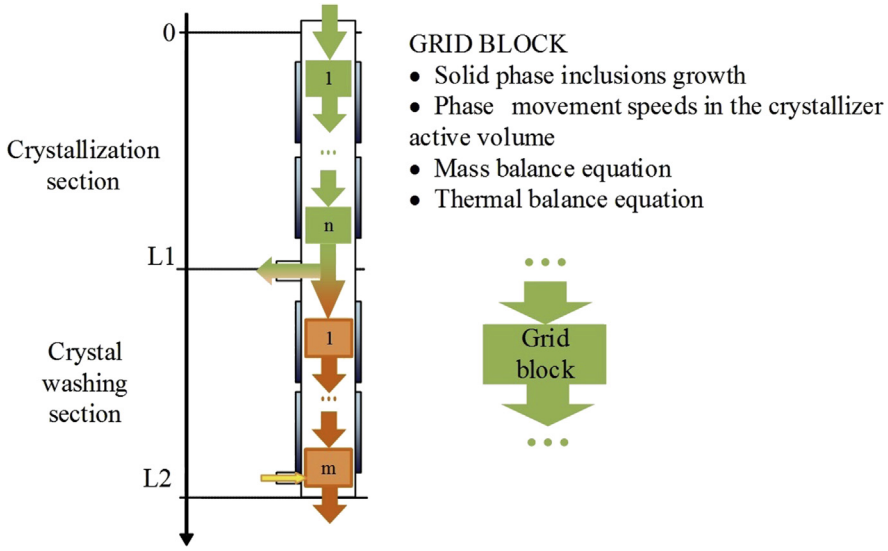

Fig. 4. Grid model of the linear crystallizer.

40 °C into the crystallization area through the batchers. As the solution drains into the column (by gravity), the working volume of the mother solution is cooled down and becomes supersaturated with the desired product. The crystal growth of the desired product occurs in the mother solution. As a consequence of differences in mass density, crystals move with the mother solution in one direction.

The nitric acid (HNO_3) solution arrives at the crystallizer washing area and is displaced by the precipitating crystals. In order to purify the surface of the crystals (by partial dissolution) the initial temperature of the washing solution and the initial concentration of the desired product are selected. The solution movement scheme is shown in Fig. 2.

Piston batchers are used to dose the solution into the crystallizer. A schematic of the batcher is shown in Fig. 3. Its design consists of a cylinder (1), within which is positioned a piston (2) that is used to batch the solution into the crystallizer. The solution is extruded when the piston is lowered (a space is left between the piston and the cylinder's walls to favor this extrusion). The solution goes into the crystallizer from the batcher through the lateral pipe (3). The drain hole (4) at the bottom of the cylinder (1) is used to wash the batcher. The piston has two holes. One hole (5) is devoted to accommodating the sensor that measures the solution level in the batcher, while the other hole (6) is used to fill the batcher with the solution. The piston is moved by a stepper motor, which

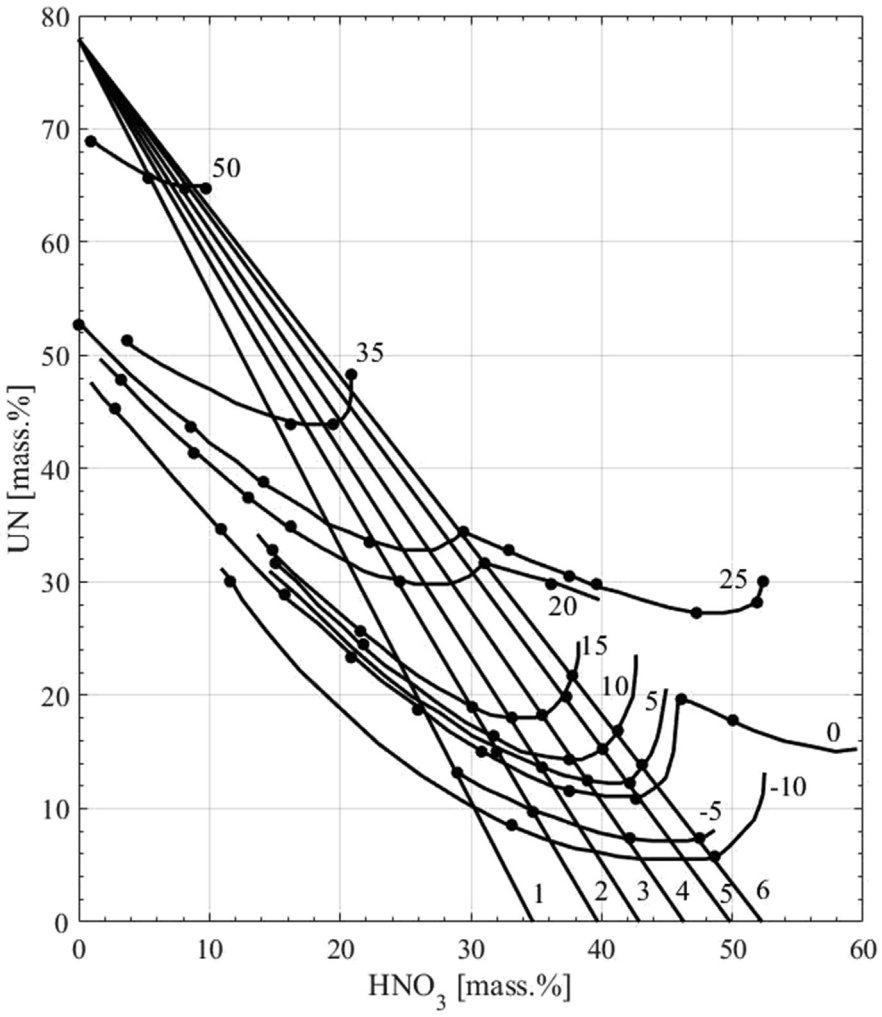

Fig. 5. Solubility of uranyl nitrate in the water solution of nitric acid at constant temperature.

is controlled by pulse frequency modulation.

It is important to highlight that the phase transition plays a key role in both the formation of the final product properties and in the heat and mass transfer. Indeed, in order to better control the crystallization process of uranyl nitrate it is necessary to have a basic understanding of the process phenomena.

3. Model

3.1. Model of uranyl nitrate crystallization process

The developed model was based on a previous work by Ochoa Bique [14], which contains equations related to heat and mass balances and the growth of the solid phase. This is a partial differential equations system that is simplified through the application of a cell-based model that, in turn, is grounded on two assumptions:

– the solution concentration of the components is the same in the whole cell; – the flow in the crystallizer is constant.

This approach allows us to reduce the description to the Cauchy form and to use the model as a control object in dynamic modeling systems, e.g., Simulink. The developed model is a cell-based model, and the linear crystallizer is divided into N interrelated, ideal mixing cells (shown in Fig. 4). Each cell includes a mass balance and heat balance equation, one related to the crystal growth and another related to the volume flow changing in the crystallizer.

The differential equations system is solved by using different algorithms included in the BzzMath library [15, 16]. The overall system behavior is characterized by the set of equations reported below.

Ochoa Bique [14] presents expression (1), which allows us to calculate the growth rate of the crystal radius. In the course of this research, changes were made to Eq. (1). As a result, crystal growth could be evaluated as follows:

$$\begin{cases} \dfrac{d\Delta R^{(i)}}{dt} = \left[K_{kr} \cdot \left(C^{0}_{UN} - C^{(i)}_{sat}\right) \cdot t_{kr}\right] / \left(0.707 \cdot t_{kr}\right) t_{kr} = \dfrac{L}{U^{(i)}_{sol}}. \end{cases} \quad (1)$$

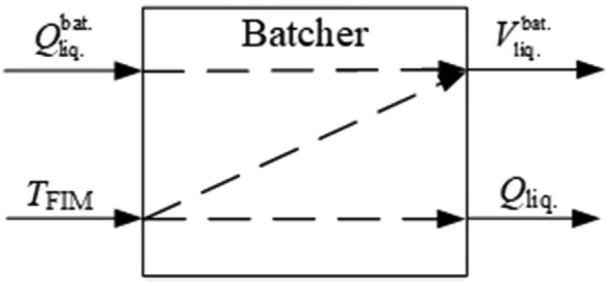

Fig. 6. Batcher information model.

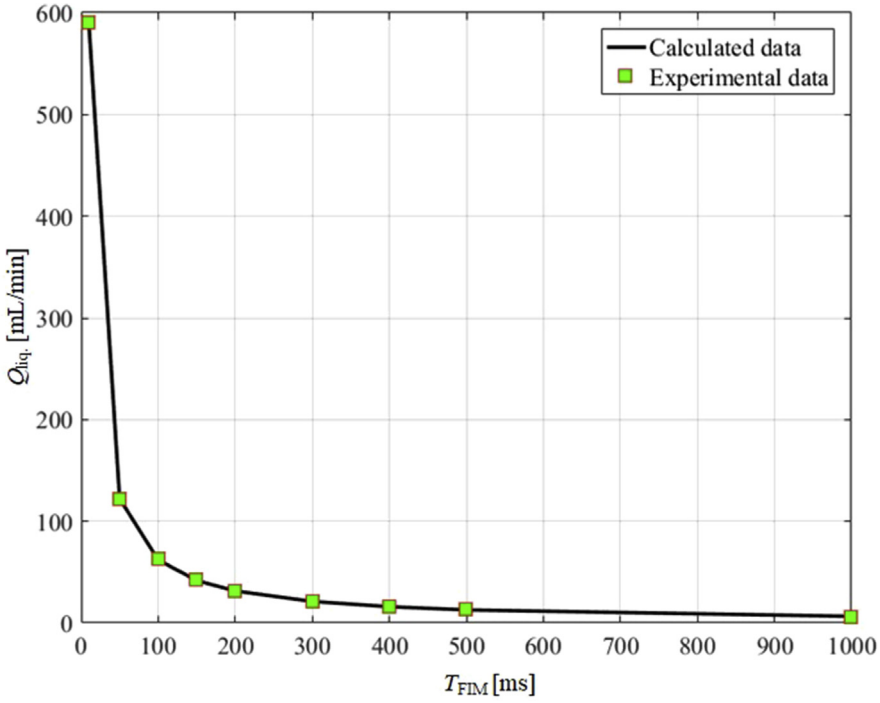

Fig. 7. Dependence between volume flow rate and pulse frequency modulation period: comparison of model prediction and experimental data.

The growth of crystals in the crystallizer occurs according to the integral law. The integral constituent was replaced by an exponential constituent with the help of an inertia link (first-order aperiodic) in the transition to the grid model of the linear crystallizer. The time constant of the inertia link (first-order aperiodic) is equal to the product $0.707 \cdot t_{kr}$.

$$\frac{dC_{UN}^{(i)}}{dt} = \frac{Q_{liq}^{(i)} \cdot ((1 - W^{(i-1)}) \cdot C_{UN}^{(i-1)} - (1 - W^{(i)}) \cdot C_{UN}^{(i)}) - (1.333 \cdot \pi \cdot n \cdot \rho_{sol} \cdot (R^3 - R_{in}^3) \cdot t_{kr}^{-1})}{V \cdot (1 - W^{(i)})}, \tag{6}$$

The coefficient 0.707 takes into account that the time constant of the inertia link is the time interval for which the response to a single step influence reaches the level 0.707 by a linear relationship.

Eqs. (2), (3), and (4) characterize the solid and liquid phase speeds and the liquid mass density, respectively:

$$U_{sol}^{(i)} = U_{liq} + \frac{2}{9}\frac{g}{v} R^{2,(i)} \left[\frac{\rho_{sol}}{\rho_{liq}^{(i)}} - 1\right], \tag{2}$$

$$U_{liq} = \frac{4}{9}\frac{Q_{liq}}{\pi D^2}, \tag{3}$$

$$\rho_{liq}^{(i)} = \left[1.023 + 2.936 \cdot 10^{-2} \cdot C_{HNO3}^{(i)}(t) + 1.313 \cdot 10^{-3} \cdot C_{UN}^{(i)}(t) - \right. \\ \left. - \left(4.681 \cdot 10^{-4} + 3.475 \cdot 10^{-5} \cdot C_{HNO3}^{(i)}(t)\right) \cdot T^{(i)}(t)\right] \cdot 10^3. \tag{4}$$

The concentration of uranyl nitrate solution is calculated as a function of nitric acid concentration through the following equation [11]:

$$C_{UN}^{(i)}(t) = A - \psi \cdot C_{HNO3}^{(i)}(t), \tag{5}$$

where $\psi = (A - C_{UN}^0)/C_{HNO3}^0$, and $A = 1/(1+\alpha) = 0.785$. The coefficient α is the mass ratio between six molecules of water and that of uranyl nitrate needed to form the uranyl nitrate hexahydrate crystal ($\alpha = 0.274$). The uranyl nitrate has limited solubility in the water solution of nitric acid. The isotherm solubility for uranyl nitrate is shown in Fig. 5 [17].

The mass balances for uranyl nitrate and nitric acid are represented by the following equations:

$$\frac{dC_{HNO3}^{(i)}}{dt} = \frac{Q_{liq}^{(i)} \cdot \left(C_{HNO3}^{(i-1)} - C_{HNO3}^{(i)}\right)}{V} \tag{7}$$

The volume fraction of the solid phase is determined as

$$W = \frac{4}{3}\pi R^3 n / V. \tag{8}$$

The heat balance for the crystallizer is described by the following subsystem of equations and represents the temperature change in internal and external heat exchange:

$$\begin{cases} \dfrac{dT_{tr}^{(i)}}{dt} = \left[a_p \cdot S_{tr} \cdot \left(T_{wall}^{(i)} - T_{tr}^{(i)}\right) - a_g \cdot S_{tr} \cdot \left(T_{tr}^{(i)} - T_{out}^{(i)}\right)\right] \Big/ \left(m_{tr}^{(i)} \cdot C_{tr}^{(i)}\right) \\ \dfrac{dT_{out}^{(i)}}{dt} = \left[a_g \cdot S_{tr} \cdot \left(T_{tr}^{(i)} - T_{out}^{(i)}\right) - M_{sum} \cdot C_{sr}^{(i)} \cdot \left(T_{out}^{(i)} - T_{in}^{(i)}\right)\right] \Big/ \left(m_{sum}^{(i)} \cdot C_{sr}^{(i)}\right) \\ M_{sum}^{(i)} = Q_{liq} \cdot \rho_{liq}^{(i)} + W^{(i)} \cdot U_{sol}^{(i)} \cdot S \cdot \rho_{sol} \\ C_{sr}^{(i)} = C_{liq}^{(i)} \cdot \left(1 - W^{(i)}\right) + C_{sol}^{(i)} \cdot W^{(i)} \\ m_{sum}^{(i)} = \rho_{liq}^{(i)} \cdot V^{(i)} \cdot \left(1 - W^{(i)}\right) + \rho_{sol} \cdot V^{(i)} \cdot W^{(i)} \end{cases} \tag{9}$$

Finally, the speed of the crystal phase in the washing area is determined by the following formulas:

$$U_{\text{sol}}^{(i)} = U_{\text{liq}} + \frac{2}{9}\frac{g}{v}R^{2,(i)}\left[\frac{\rho_{\text{sol}}}{\rho_{\text{liq}}^{(i)}} - 1\right] - U_{\text{pr}},$$
$$U_{\text{pr}} = \frac{Q_{\text{pr}}}{S} + U_{\text{sol}}^{(i)}(t)\sqrt{\frac{\rho_{\text{sol}}}{\rho_{\text{liq}}^{(i)}}}. \quad (10)$$

3.2. Model of the crystallizer supply system

The aim of the crystallizer supply system is to keep a constant level of the mother solution in the crystallizer for its smooth and efficient operation. The feeding of the mother solution is carried out by the two piston batchers described earlier (Fig. 3). In order to develop a suitable model, we created an information model for the batchers was created (Fig. 6).

The filling speed of the mother solution depends on the inlet volume flow into the batcher. The outlet solution flow depends on the lowering speed of the piston, which, in turn, is related to the period of the pulse frequency modulation. Therefore, the filling speed of the batcher and the pulse frequency modulation period are input variables of the model. The output variables are the volume of the nitric acid solution of U-Pu-Np in the batcher, and the volume flow of the solution at the outlet of the batcher.

For the purpose of our simulations, it is necessary to calculate, at every time step, the variation of the solution's volume in the batcher:

$$\frac{dV_{\text{liq.}}^{\text{bat.}}}{dt} = Q_{\text{liq.}}^{\text{bat.}} - Q_{\text{liq.}}. \quad (11)$$

The volume flow of the solution depends on both the flow rate and the section area of pipe 6 (see Fig. 3), through which the batcher is filled. The volume flow and the section area of pipe 6 are determined by the following formulas:

$$Q_{\text{liq.}}^{\text{bat.}} = v_{\text{liq.}}^{\text{bat.}} \cdot S_{\text{b.p.6}}, \quad (12)$$

$$S_{\text{b.p.6}} = \pi \cdot R_{\text{b.p.6}}^2. \quad (13)$$

As mentioned earlier, the outlet volume flow depends on the piston speed. However, the piston is moved by a stepper motor, which is controlled by a pulse frequency modulation. The dependency between the modulation period and the volume flow of the solution is non-linear. The stepper motor makes one step after one pulse produced by frequency modulation. One step is equal to 0.01 mm of piston movement.

The number of steps taken by the stepper motor within 1 s is determined by equation (14), and, consequently, the volume flow of the outlet solution is evaluated with formula (15).

$$N_{\text{step}} = \frac{1}{T_{\text{FIM}}} \quad (14)$$

$$Q_{\text{liq}} = N_{\text{step}} \cdot \Delta h_{\text{piston}} \cdot S_{\text{piston}} \quad (15)$$

The area of the piston base is calculated by expression (16).

$$S_{\text{piston}} = \pi \cdot r_{\text{piston}}^2 - \pi \cdot r_{\text{hole5}}^2 - \pi \cdot r_{\text{hole6}}^2 \quad (16)$$

Moreover, the volume flow of the outlet solution was calculated at different values of pulse frequency modulation period. As shown in Fig. 7, the results of these simulations are in very good agreement with the experimental data obtained the “Proryv” project.

The variation of component concentrations in the batcher are calculated using the following expression:

$$\frac{dC_{\text{i}}}{dt} = \frac{C_{\text{i}}^{\text{bat.}} \cdot Q_{\text{liq.}}^{\text{bat.}} - C_{\text{i}} \cdot Q_{\text{liq.}}}{V_{\text{liq.}}^{\text{bat.}}}. \quad (17)$$

The operation of the batcher can be then described by the below equation system:

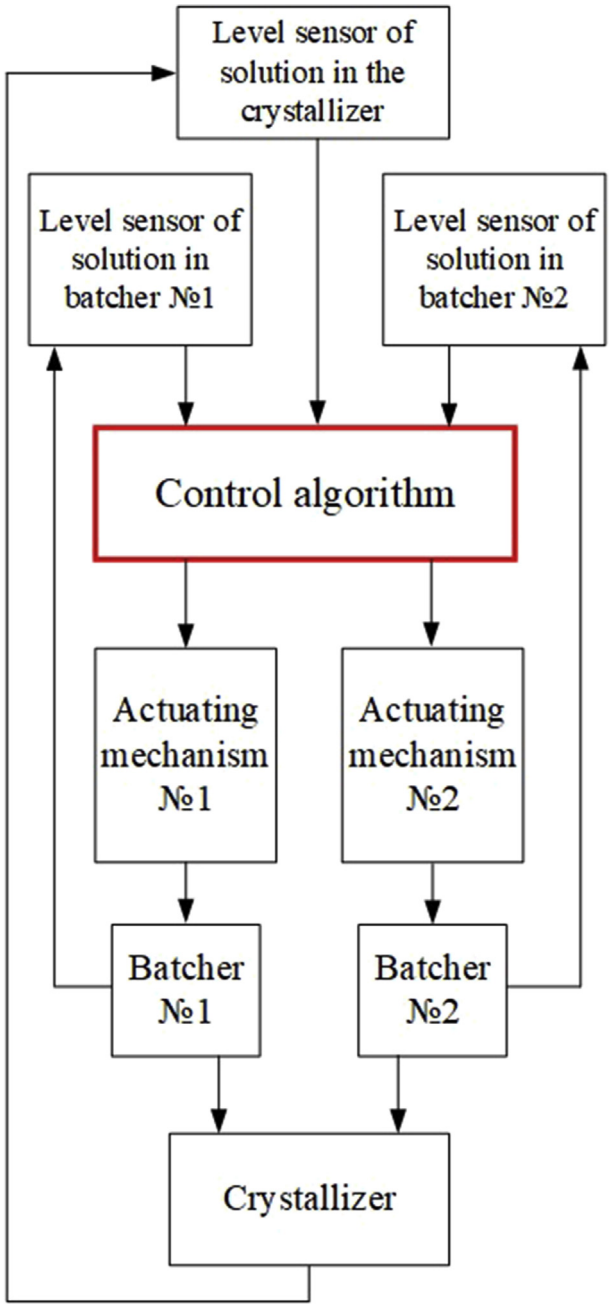

Fig. 8. Structural scheme of proposed automatic control system.

$$\begin{cases} \dfrac{dV_{\text{liq.}}^{\text{bat.}}}{dt} = Q_{\text{liq.}}^{\text{bat.}} - Q_{\text{liq.}} \\ Q_{\text{liq.}}^{\text{bat.}} = v_{\text{liq.}}^{\text{bat.}} \cdot S_{\text{b.p.6}} \\ Q_{\text{liq.}} = N_{\text{step}} \cdot \Delta h_{\text{piston}} \cdot S_{\text{piston}} \\ \dfrac{dC_{\text{i}}}{dt} = \dfrac{C_{\text{i}}^{\text{bat.}} \cdot Q_{\text{liq.}}^{\text{bat.}} - C_{\text{i}} \cdot Q_{\text{liq.}}}{V_{\text{liq.}}^{\text{bat.}}} \end{cases}. \quad (18)$$

We solve the equation system (18) using the initial conditions:

$$\begin{cases} V_{\text{liq.}}^{\text{bat.}}(0) = 0 \\ C_{\text{i}}(0) = 0 \end{cases}. \quad (19)$$

In the following section we see how the control algorithm for the crystallizer supply system was created using the aforementioned model.

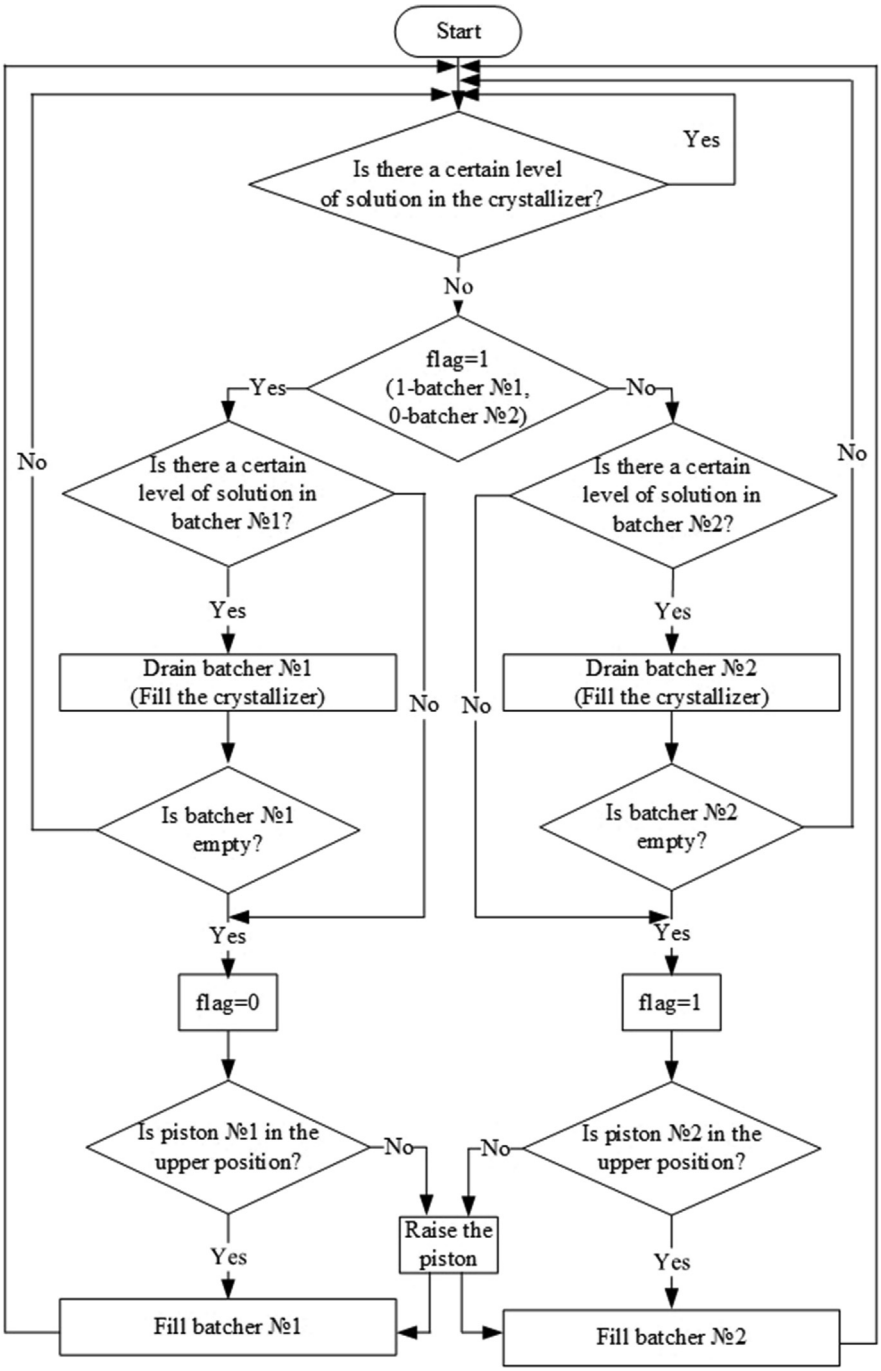

Fig. 9. Supply system control algorithm.

3.3. Development of the algorithm for process control

Two batchers, working in an alternating way, were used for continuous filling of the crystallizer: one injected the mother solution into the crystallizer while the other was filled by the solution. The structural scheme of the proposed automatic control system of the crystallizer is shown in Fig. 8.

The actuating mechanisms are the stepper motors, which are controlled by pulse frequency modulation. The solution level in the crystallizer is measured by level sensors. When the solution level is lower than the set point, the control system sends a signal to the stepper motor to fill the crystallizer. From a modeling standpoint, at the beginning, batchers are assigned with a tag number (i.e., 0 for one batcher and 1 for the other one), and the same batcher is used to feed the crystallizer. Then, there is a check to fill the batcher to the desired level, and the solution volume control for the batcher is carried out by level sensors. When the selected batcher contains enough solution, it starts to fill the crystallizer. When the batcher is empty, the other batcher begins to fill the crystallizer. In order to fill the batcher with the mother solution, the batcher's piston is raised to the top position. Then, the fully filled batcher waits until the second batcher is empty, and then the process starts over again. A conceptual block diagram of the described control algorithm is shown in Fig. 9. This was the result of research on crystallization process sensitivity to solution level in a crystallizer based on numerical experiments.

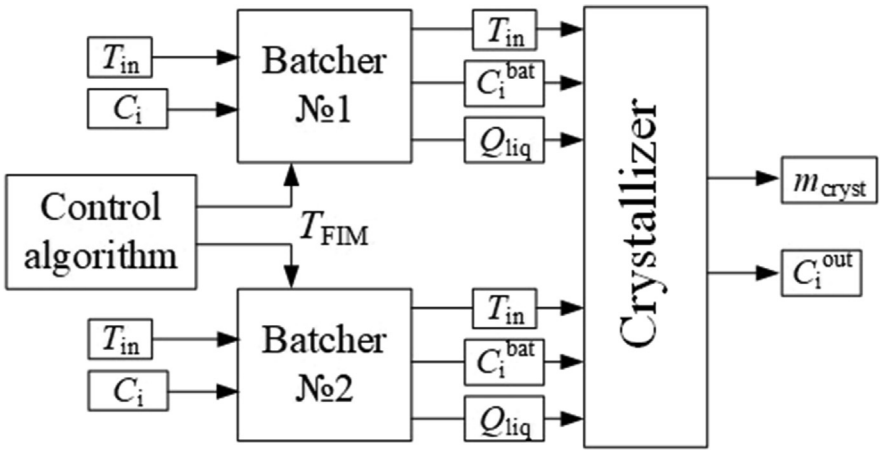

Fig. 10. Information structure of crystallizer.

Table 1
Variables.

Variable	Name		Initial value
Q_{liq}	Inlet solution flow rate at crystallizer	[rel. un.]	1
C_i^{bat}	Outlet mass fraction of the metal in the solution	[rel. un.]	
C_i	Mass fraction of the metal in mother solution	[rel. un.]	1
T_{in}	Inlet solution temperature	[°C]	40
T_{FIM}	Period of pulse frequency modulation	[ms]	300
m_{cryst}	Outlet mass flow of crystals	[rel. un.]	
C_i^{out}	Mass fraction of the metal in the mother–washing solutions	[rel. un.]	

4. Experimental

This section presents simulation results of the crystallization process using the Simulink (commercial) application. The information structure of the crystallizer is shown in Fig. 10, and Table 1 presents the related variables. The crystallization area was divided into 100 cells in order to improve the sensitivity of the model to the possible change in solution level in the crystallizer.

4.1. Results

Simulation results for the crystallization process are shown in Fig. 11.

These graphs show the crystallizer's performance and solution level in relative units. The product's mass flow at the crystallizer outlet is determined as follows:

$$m_{cryst}(t) = U_{sol}(t) \cdot S \cdot \rho_{sol} \cdot W. \quad (20)$$

It is worth noting from Fig. 11 that there is a delay time of about 0.565 h in the mass flow rate production. That is the time needed to fill the batchers at the beginning of the experiment. Diagrams representing the filling and emptying dynamic of the batchers during operation are shown in Fig. 12. As can be noticed, the designed algorithm for process control performs correctly as it keeps the desired level of the mother solution in the crystallizer practically constant (i.e., around 1).

As mentioned earlier, accurately measuring the solution level in the crystallizer might be practically difficult due to the impossibility of precisely locating the sensor(s) in the crystallizer body. This is why there is a static measurement error besides the signal noise of the sensor itself. The static measurement error can be explained by the fact that the ultrasonic sensor measures the solution level by passing the signal through the crystallizer. As a result, the signal is distorted and the sensor measures might be incorrect or imprecise.

A series of virtual experiments were performed in order to study the crystallization process stability with static error and additive noise. A static error is defined as the difference between the measured value and the true value of the quantity. Additive noise (additive error) is an interference added to the signal to mimic the effect of many random processes that occur in nature. The simulations were performed by adding static and additive errors to the sensor signal, and the results are presented in Fig. 13. As can be seen, the static error decreases the crystallizer's performance. Additive interference and static error cause fluctuation of the crystallizer's output variable. However, the additive interference could be easily removed by using a filter.

A series of virtual experiments were performed in order to study the crystallizer's performance related to the solution level in the crystallizer.

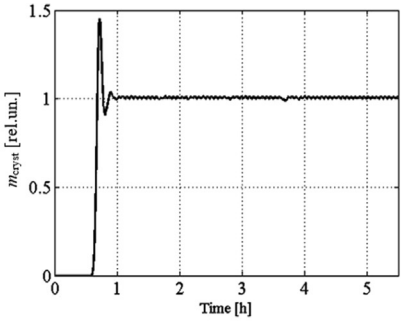

(a) Outlet mass flow of products at crystallizer

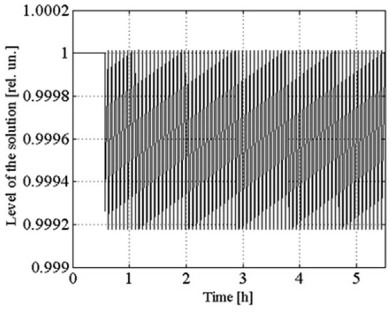

(b) Mother solution level in crystallizer

Fig. 11. Simulation results for the crystallization process in the linear crystallizer.

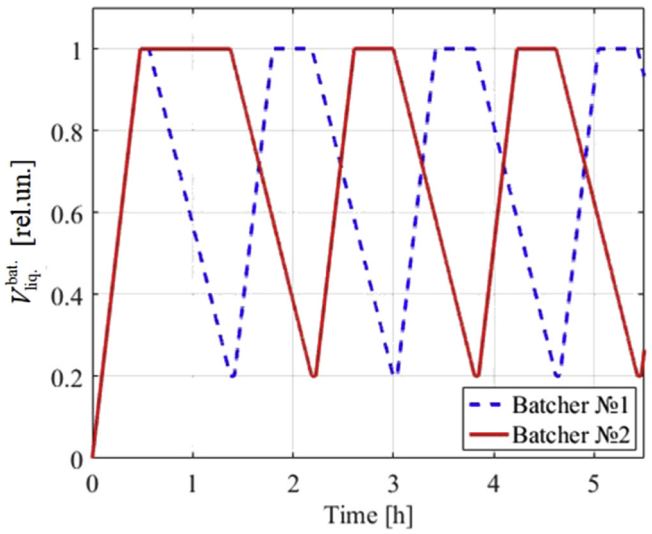

Fig. 12. Diagrams of batchers filling and emptying.

Static error was added to the sensor signal. The level sensor gave a signal that overestimated the real level of the solution. Therefore, the mother solution level in the crystallizer was lower than the nominal one, which is equal to 1 relative units (rel. un.). For instance, a static error of 6.7%–93.3% of the nominal value on the solution level means that the level of the mother solution in the crystallizer is rated at 0.067–0.933 rel. un. The results of some experiments are shown in Fig. 14 and Table 2.

The increasing static error causes the decrease in the mother solution level in the crystallizer, and, in turn, the decrease in outlet mass flow rate of crystals. As a result, the performance of the crystallizer decreases

Table 2
Experimental results.

Exp. №º	Static error of measuring [%]	Crystallizer performance [%]	Flow rate of mother solution [%]
1	6.7	91.6	95.8
2	13.3	82.1	91.5
3	20.0	73.2	87.1
4	26.7	64.1	82.6
5	33.3	55.6	77.9
6	40.0	49.4	73.1
7	46.7	41.6	68.1
8	53.3	33.7	62.9
9	60.0	27.5	57.4
10	66.7	21.3	51.6
11	73.3	16.0	45.5
12	80.0	10.7	38.8
13	86.7	5.4	31.7
14	93.3	1.0	24.2

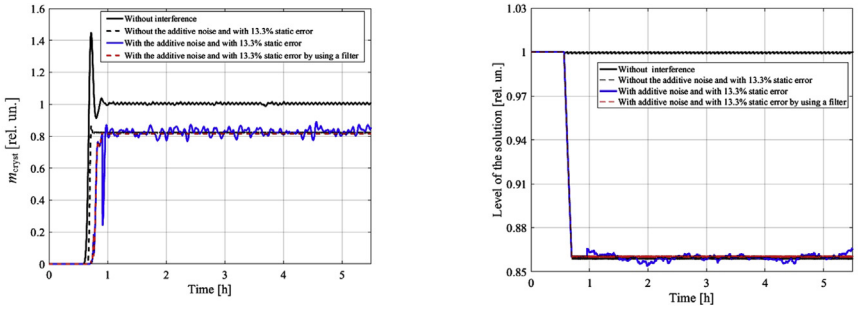

(a) Mass flow of products at crystallizer outlet (b) Mother solution level in crystallizer

Fig. 13. Simulation results for the crystallization process with static error and additive noise.

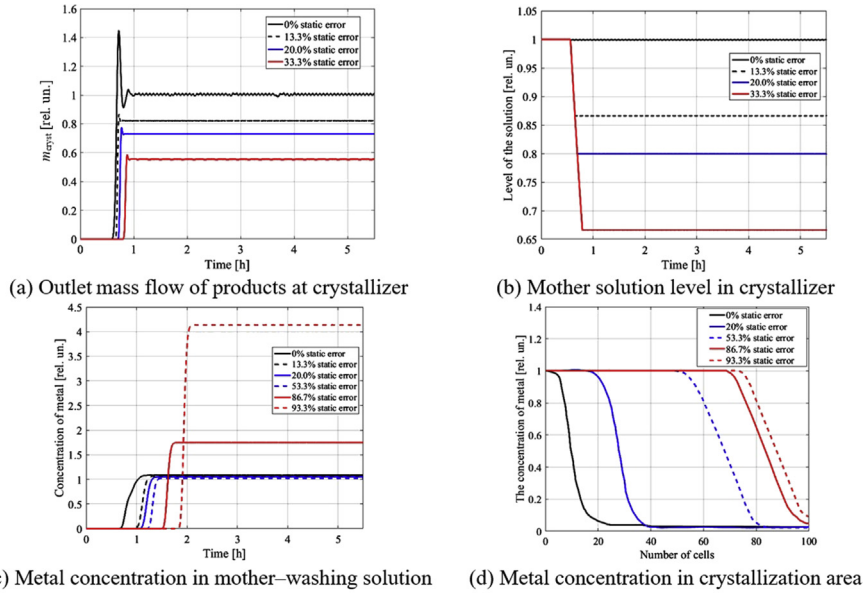

(a) Outlet mass flow of products at crystallizer (b) Mother solution level in crystallizer

(c) Metal concentration in mother–washing solution (d) Metal concentration in crystallization area in cells

Fig. 14. Simulation results for the crystallization process with static error.

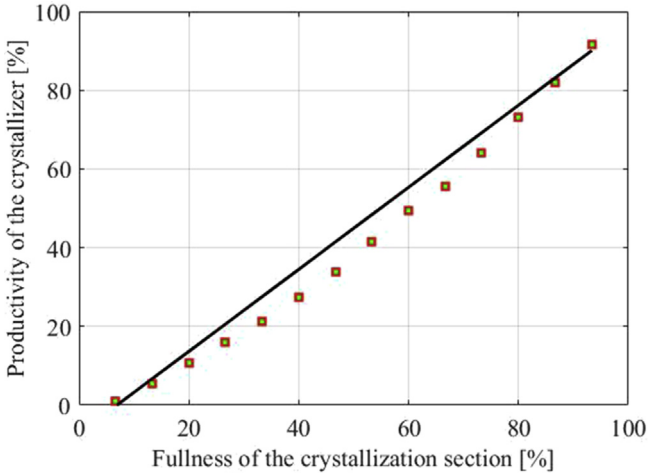

Fig. 15. Relationship between the crystallizer's performance and the level of the mother solution in the crystallizer area.

(Fig. 14). However, the metal concentrations in the mother–washing solutions are not significantly reduced if the static error does not exceed the 86.7% of the solution level. This behavior can be explained by considering that the mother–washing solutions' flow rates are reduced with the decrease in crystallization area fullness. If the static error exceeds 86.7%, a significant part of the desired product comes out of the crystallizer with the mother–washing solutions (Fig. 14). To better understand the effect of the level of the mother solution in the crystallizer section (i.e., the fullness) on the productivity of the crystallizer, the experimental data presented in Table 2 is charted to create Fig. 15.

As Fig. 15 shows, there is a non-linear relationship between the crystallizer's fullness and its performance. What influences the crystallizer's performance is both its height and fullness. More specifically, the following correlation was created to calculate the crystallizer's performance:

$$m_{cryst} = 0.004591 \cdot lev_{liq}^2 + 0.5834 \cdot lev_{liq} + 3.033. \quad (21)$$

Through Eq. (21) we found that the crystallizer's performance did not reduce by more than 5% when the error in the solution level in the crystallization area did not exceed 4%.

According to the simulations performed, the change in solution level in the crystallization area leads to an insignificant change in mother–washing solutions' temperature at the crystallizer outlet. This behavior could be due to the fact that the maximum filling of the crystallization area leads to a maximum of the heat exchange area. However, the solution residence time is lower, and this can be ascribed to the increase in flow rate of the mother–washing solutions. At partial filling of the crystallization area, the heat exchange area is lower, and the outlet flow rates of the mother–washing solutions of the crystallizer arer reduced; this leads to an increase in residence time of the solution in the crystallizer.

5. Conclusion

The aim of the work presented in this manuscript was to create a mathematical model for a linear crystallizer and the associated piston batcher(s). In addition, a control algorithm for the supply system to support operability was developed. This algorithm allowed us to maintain a specified level of mother solution in the crystallization area and provides an asynchronous operation mode for the batchers. The developed mathematical model was used to perform simulations. As a result of the experiments, a non-linear relationship between the crystallizer fullness and its performance was identified. It was shown that a liquid phase level reduction to 86.7% does not lead to a significant ejection of target components. Furthermore, it was shown that a significant part of the target product comes out from the crystallizer with the mother and washing solution when the level in the crystallizer is less than 86.7%. Lastly, an expression for calculating the performance of the crystallizer was proposed. This expression allowed us to understand that the accuracy of the liquid phase level (to avoid the crystallizer's performance decreasing by more than 5%) should be in the range of ±4% of the crystallization section height.

Declarations

Author contribution statement

Igor Nadezhdin: Conceived and designed the experiments; Performed the experiments; Wrote the paper.

Alexandr Gozhimov: Performed the experiments; Wrote the paper.

Alexey Goryunov: Conceived and designed the experiments; Analyzed and interpreted the data; Contributed reagents, materials, analysis tools or data.

Simone Colombo: Analyzed and interpreted the data; Wrote the paper.

Flavio Manenti: Conceived and designed the experiments; Analyzed and interpreted the data.

Funding statement

This work was supported as a part of the project 8.3079.2017/4.6 of the Federal government-sponsored program «Science».

Competing interest statement

The authors declare no conflict of interest.

Additional information

No additional information is available for this paper.

References

[1] J.J. Taylor, The nuclear power bargain, Issues Sci. Technol. 20 (3) (2004) 41–47.
[2] C. Lindenberg, M. Krättli, J. Cornel, M. Mazzoti, J. Brozio, Design and optimization of a combined cooling/antisolvent crystallization process, Cryst. Growth Des. 9 (2009) 1124–1136.
[3] E. Henrich, H. Schmieder, K. Ebert, Combination of TBP extraction and nitrate crystallization for spent nuclear fuel reprocessing, Inst. Chem. Eng. Symp. Ser. 103 (1987) 191–205.
[4] J.S. Shepherd, M. Fairweather, P.J. Heggs, B.C. Hanson, Mathematical modelling of the pre-oxidation of a uranium carbide fuel pellet, Comput. Chem. Eng. 83 (2015) 203–213.
[5] T. Chikazawa, T. Kikuchi, A. Shibata, T. Koyama, S. Homma, Batch crystallization of uranyl nitrate, J. Nucl. Sci. Technol. 45 (2008) 582–587.
[6] T. Takata, Y. Koma, K. Sato, M. Kamiya, A. Shibata, K. Nomura, H. Ogino, T. Koyama, S.I. Aose, Conceptual design study on advanced aqueous reprocessing system for fast reactor fuel cycle, J. Nucl. Sci. Technol. 41 (2004) 307–314.
[7] S. Homma, J.I. Ishii, T. Kikuchi, T. Chikazawa, A. Shibata, T. Koyama, J. Koga, S. Matsumoto, Flowsheet study of U-Pu co-crystallization reprocessing system, J. Nucl. Sci. Technol. 45 (2008) 510–517.
[8] S. Homma, J.I. Ishii, J. Koga, S. Matsumoto, T. Kikuchi, T. Chikazawa, A. Shibata, Flowsheet analysis of U-Pu co-crystallization process as a new reprocessing system, in: International Conference on Nuclear Engineering, Proceedings, ICONE, 2006.
[9] S.A. Rocha, R. Guirardello, An approach to calculate solid–liquid phase equilibrium for binary mixtures, Fluid Phase Equilib. 281 (2009) 12–21.
[10] F.I. Tumakaka, I.V. Prikhodko, G. Sadowski, Modeling of solid–liquid equilibria for systems with solid-complex phase formation, Fluid Phase Equilib. 260 (2007) 98–104.
[11] S. Veselov, V. Volk, V. Kasheev, T. Podimova, E. Posenitskiy, Mathematic simulation of crystallization refining process of spent nuclear fuel reprocessing desired products in linear crystallizer, Adv. Mater. Res. 1084 (2015) 666–672.
[12] E.R. Abasheva, H.K. Chan, E.M. Koltsova, Cellular automata for simulation of producing process of Fe – Nanothreads, in: CHISA 2006 – 17th International Congress of Chemical and Process Engineering, 2006.
[13] A.O. Ochoa Bique, A.G. Goryunov, Simulation of the uranium crystallization process using cellular automata, Adv. Mater. Res. 1084 (2015) 72–76.

[14] A.O. Ochoa Bique, A.G. Goryunov, F. Manenti, A comparison of simulation techniques for uranium crystallization process, Chem. Eng. Trans. 43 (2015) 793–798.
[15] G. Buzzi-Ferraris, F. Manenti, BzzMath: library overview and recent advances in numerical methods, Comp. Aided Chem. Eng. 30 (2012) 1312–1316.
[16] F. Manenti, I. Dones, G. Buzzi-Ferraris, H.A. Preisig, Efficient numerical solver for partially structured differential and algebraic equation systems, Ind. Eng. Chem. Res. 48 (2009) 9979–9984.
[17] S.N. Veselov, V.I. Volk, V.A. Kasheev, T.V. Podymova, E.A. Posenitskiy, Mathematical simulation of the crystallization process in a continuous linear crystallizer, J. Eng. Phys. Thermophys. 90 (2017) 140–150.